Available online at www.sciencedirect.com
ScienceDirect
Journal of Sound and Vibration 307 (2007) 849–864
JOURNAL OF SOUND AND VIBRATION
www.elsevier.com/locate/jsvi

Passive hybrid technique for the vibration mitigation of systems of interconnected stays

Luca Caracoglia[a,*], Nicholas P. Jones[b]

[a]Department of Civil and Environmental Engineering, Northeastern University, Boston, MA 02115, USA
[b]G.W.C. Whiting School of Engineering, The Johns Hopkins University, Baltimore, MD 21218, USA

Received 9 January 2006; received in revised form 5 October 2006; accepted 18 July 2007
Available online 24 August 2007

Abstract

The problem of stay oscillation mitigation in cable-stayed bridges, usually induced by wind or wind and rain, may require the introduction of passive devices, such as dampers on individual stays or the use of transverse restrainers (cross-ties). The damper performance is often affected by the geometrical constraints of the bridge deck that limit the installation of such devices to locations very close to the end of the cable. On the other hand, cross-ties are generally incapable of direct energy dissipation. Therefore, the authors have proposed and analyzed a hybrid passive system in which the advantages of both techniques are applied to the oscillation mitigation of complex interconnected systems with multiple external dampers at the deck level, in correspondence with the cross-tie lines.

This paper summarizes the relevant findings of a research program involving the authors' efforts focused on the in-plane free-vibration analysis of stay-cable systems. This research is also based upon some recent results associated with the analytical solution of a taut-cable with two attached viscous dampers. These findings are initially extended to a simplified network with reduced number of connectors and one damper, for which the derivation of analytical solution is still possible. Subsequently, an existing multistay multidamped arrangement on a real bridge is considered, in which a fully numerical approach is required. The modal behavior is compared to the simplified examples, also enabling the interpretation of the results in the context of more general guidelines for potential future application.

1. Introduction

A quite common strategy for the mitigation of wind and wind–rain induced oscillation [1] is the use of transverse steel-wire cables, called cross-ties, which contribute to a general increment in the in-plane stiffness of the system and transform the individual cables into a network [2–5]. When cross-ties only are employed, frequencies corresponding to in-plane modes of the longest cables, more vulnerable to external excitation, are usually tuned to higher values by the presence of the restrainers, significantly reducing the risk of oscillation. In addition, the in-plane fundamental modes of the modified system, acting as a whole entity, generally posses a very large modal mass compared to each individual cable, as recently shown by the authors through an

*Corresponding author. Tel.: +1 617 373 5186; fax: +1 617 373 4419.
E-mail address: lucac@coe.neu.edu (L. Caracoglia).

0022-460X/$ - see front matter © 2007 Elsevier Ltd. All rights reserved.
doi:10.1016/j.jsv.2007.07.022

analytically derived method based upon the solution to free-vibration problem for cable networks in terms of taut-cable theory [5,6].

However, some limitations are also evident such as, for example, the fact that this system is incapable of direct energy dissipation, the ineffectiveness of the suppression of out-of-plane modes due to the limited influence of the restrainers, and the presence of a large number of higher-frequency localized modes, which are usually difficult to control. This study was motivated by the fact that such complex systems of interconnected stays can still experience high levels of vibration during severe wind events, as observed during full-scale measurements on an existing system [6].

Since the stays are inherently low-damping systems, the addition of mechanical devices has been traditionally proposed in the literature for mitigation purposes, in which dampers are connected to each individual cable (cable-damper system). One of the first studies simulated of the response associated with the installation of a passive viscous damper on a stay [7] through taut-cable theory [8]. This study was followed by the numerical derivation of an optimal "universal estimation curve" for a damper located near the end of the cable [9], subsequently extended in Refs. [10,11] by considering three-dimensional and sag effects. Recently, a closed-form solution to the problem of a viscous damper attached to a taut-string was developed [12,13], in which a general analytical framework for the free-vibration solution in terms of complex-frequency analysis was introduced. The problem of a shallow cable with viscous damper by including sag effects and the presence of a coupled spring–mass–damper system was considered in Ref. [14], while the use of semi-active devices was also proposed to overcome some of the limitations of passive devices located close to the stay end (e.g., [15,16]).

In this study, the authors propose a hybrid solution that combines the advantages of the network with the benefits associated with the possibility combining the effects of the cross-ties and external dampers directly connected to the deck in order to address—in part—the limitations of a traditional network. Similar hybrid configurations were recently discussed in Ref. [17], while the use of dampers installed between stays at internal locations was investigated in Refs. [18–20], confirming the interest in the study of these systems for vibration reduction as an alternative to cable-damper systems. The analysis framework developed for a simplified linear damper-cable system is incorporated into the analytical method, developed for the study of in-plane cable networks without damping devices [6]. The derivation of a closed-form solution was only possible for examples with a limited number of either stays, connectors or dampers. A numerical technique was required for all other cases.

Therefore, the dynamic behavior of a simplified cable network is initially analyzed, for which mode identification can be carried out in closed form; results are later used for the response interpretation on a larger system. In the second part of the paper, an application to real multistay systems is presented, based upon the observations derived from the first part and applied to the study of an existing network, currently installed on a cable-stayed bridge and including the installation of one or more dampers. The solution is also compared with the case associated with two dampers on a single stay [21], recently indicated as a potential way of improving the performance of stay-damper arrangements in the presence of geometric configuration limitations. The characterization of the system modal performance before and after the introduction of the restrainers is carefully considered.

2. Cable dynamics

A linear analytical method for the in-plane free-vibration analysis of cable networks in the absence of external dissipation devices was developed in Ref. [6]. In this study, the original formulation was modified to allow for the presence of external discrete external dampers located in correspondence with the restrainers. Differences with respect to the previous work are summarized in this section.

The cable network configuration is simulated by a set of parallel cables (Fig. 1), interconnected by means of restrainers on occasion extended to ground or connected to the deck through damping devices. The generic jth cable ($j = 1,\ldots,n$) in Fig. 1 is divided into m_j segments (with $m_1,\ldots,m_j,\ldots,m_n$ usually different for each cable). The free-vibration problem of each pth element of the jth cable (with $j = 1,\ldots,n$ and $p = 1,\ldots,m_j$) is solved (linear taut-string theory [8]) as

$$H_j \partial^2 y_{jp} \Big/ \partial x_{jp}^2 = \mu_j \partial^2 y_{jp} \Big/ \partial t^2 \tag{1}$$

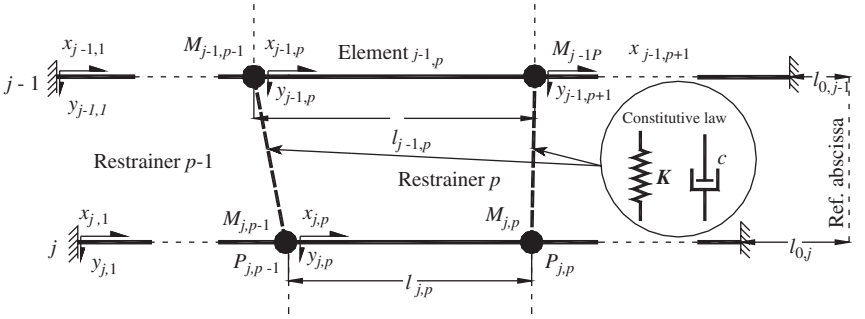

Fig. 1. Generalized cable network configuration.

with $y_{jp}(x_{jp},t)$ time- and position-dependent transverse displacement along the segment jp between nodes $P_{j,p-1}$ and $P_{j,p}$, L_j cable length, H_j cable tension and μ_j mass per unit length. In contrast with the previous work, the motion of each element must be assumed as $y_{jp}(x_{jp},t) = \mathrm{Re}[Y_{jp}(x_{jp})e^{i\omega t}]$, in which ω is a complex circular frequency [12] due to the presence of the dampers, and reducing Eq. (1) to

$$H_j \, \mathrm{d}^2 Y_{jp} \Big/ \mathrm{d}x_{jp}^2 + \mu_j \omega^2 Y_{jp} = 0. \tag{2}$$

A solution in terms of trigonometric functions:

$$Y_{jp}(x_{jp}) = A_{j,p} \sin\left(\gamma\pi L_j^{-1} f_j x_{jp}\right) + B_{j,p} \cos\left(\gamma\pi L_j^{-1} f_j x_{jp}\right) \tag{3}$$

is adopted, with $A_{j,p}$ $B_{j,p}$ complex amplitudes and $f_j = \omega_{01}/\omega_{0j}$ jth cable frequency ratio. The quantity $\omega_{01} = \pi/L(H_1/\mu_1)^{0.5}$ is the fundamental real circular frequency of a reference cable (usually $j = 1$) and $\gamma = \alpha + i\beta$ represents a normalized complex frequency ($i = \sqrt{-1}$) such that $\omega = \gamma\omega_{01}$. The length of each jp segment is $l_{j,p}$ and $\xi_{j,p} = l_{j,p}/L_j$. The complex variable ω (or γ) can be equivalently expressed in terms of its real and imaginary parts, as $\omega = \omega_{01}(\alpha + i\beta) = \tilde{\omega}\sqrt{1-\eta^2} + i\eta\tilde{\omega}$ with $\tilde{\omega} = \omega_{01}\mathrm{norm}[\gamma]$. The damping ratio $0 \leqslant n \leqslant 1$ is computed as $\eta = [\zeta/(1+\zeta)]^{0.5}$ with $\zeta = (\beta/\alpha)^2$.

Eq. (3) are subsequently solved for the unknown amplitudes $A_{j,p}$ and $B_{j,p}$ by means of a set of internal and external compatibility, continuity and equilibrium equations for a network with one or more external viscous dampers connected to the deck, i.e.,

$$B_{j,1} = 0 \quad A_{j,m_j} \sin\left(\gamma\pi f_j \xi_{j,m_j}\right) + B_{j,m_j} \cos\left(\gamma\pi f_j \xi_{j,m_j}\right) = 0 \quad \text{with} \quad j = 1,\ldots,n, \tag{4,5}$$

$$A_{j,p_j} \sin\left(\gamma\pi f_j \xi_{j,p_j}\right) + B_{j,p_j} \cos\left(\gamma\pi f_j \xi_{j,p_j}\right) - B_{j,p_j+1} = 0 \quad \text{with} \quad j = 1,\ldots,n, p_j = 1,\ldots,m_j, \tag{6}$$

$$\hat{K}_{j,p}\left(B_{j+1,p+1} - B_{j,p+1}\right) = \sum_{k=1}^{j} \gamma\pi H_1 L_1^{-1} \sigma_{k,j}^{p} \left\{ \begin{array}{c} v_k\left[A_{k,p} \cos\left(\gamma\pi f_k \xi_{k,p}\right) - B_{k,p} \sin\left(\gamma\pi f_k \xi_{k,p}\right)\right. \\ \left. -A_{k,p+1}\right] - \gamma\pi\chi_{k,p} B_{k,p+1} \end{array} \right\}$$
$$\text{with} \quad p = 1,\ldots,\tilde{m}-1, j = 1,\ldots,(g_p - 1), \quad \tilde{m} = \max[g_p], \tag{7}$$

$$i\rho_{D_p} B_{g_p,p+1} = \sum_{j=1}^{g_p} \sigma_{j,g_p}^{p} \left\{ v_j \left[A_{j,p} \cos\left(\gamma\pi f_j \xi_{j,p}\right) - B_{j,p} \sin\left(\gamma\pi f_j \xi_{j,p}\right) - A_{j,p+1} \right] - \gamma\pi\chi_{j,p} B_{j,p+1} \right\},$$
$$\text{with} \quad p = 1,\ldots,\tilde{m}-1. \tag{8}$$

External boundary conditions are enforced through Eqs. (4) and (5), the continuity between consecutive segments on the same stay through Eq. (6), and internal and global force equilibrium through Eqs. (7) and (8). Inertial terms are introduced to account for the mass of the secondary system, represented through lumped elements $M_{j,p}$ at each node $P_{j,p}$; linear spring elements are employed to simulate internal cross-tie segments.

The variable g_p denotes the maximum number of connected cables for the pth cross-tie. The quantity $v_j = [(\mu_j H_j)/\mu_1 H_1]^{0.5}$ is a mass-tension reduction factor, as it accounts for the relative reduction of mass and tension of each cable with respect to the reference stay, $\chi_{j,p} = M_{j,p}/(\mu_1 L_1)$ and $\hat{K}_{j,p} = K_{j,p}[\sin(\psi_{j,p})]^2$ for an inclined restrainer with stiffness $K_{j,p}$. The non-parallel three-dimensional orientation of stays and restrainers (Eqs. (8) and (9)) is considered through $\sigma^p_{k,j} = \Pi_{q=k}^{j-1} \sin\hat{\psi}_{q,p}/\sin\psi_{q,p}$ ($\sigma_{j,j}{}^p = 1$), with $\psi_{q,p}$ and $\hat{\psi}_{q,p}$ relative inclinations of each cross-tie segment qp with respect to stays q and $q+1$, respectively.

Global force equilibrium equations at each cross-tie (Eq. (8)) account for the presence of external viscous dampers connected to the deck in correspondence with the restrainers. Each unit with viscous coefficient c_{D_p} and dimensionless damping parameter $\rho_{D_p} = c_{D_p}(H_1\mu_1)^{-0.5}$ is installed (if present) on the pth restrainer below the lower cable.

A homogeneous system of $2r = 2\Sigma m_j$ equations is derived as $\mathbf{S\Phi} = \mathbf{0}$, in which the complex matrix $\mathbf{S}$ is composed by a set of algebraic nonlinear relationships as a function of γ. The vector $\mathbf{\Phi} \in \mathbb{C}^{2r}$ contains the unknowns $A_{j,p}$ and $B_{j,p}$. This system is numerically solved for γ, associated with the condition $\det[\mathbf{S}] = 0$, as an eigen-value–eigen-vector problem. Each mode is generally characterized by two limiting cases with real eigen-values ($\beta \equiv 0$) and no dissipation: $\rho_p = 0$ i.e., *undamped* solution in which no dampers to ground are present and $\rho_p \to \infty$, i.e., *locked* dampers equivalent to a rigid connection to the deck. Between these two cases the mode is complex and usually *underdamped,* with an oscillatory eigen-function prevailing and $\eta \leqslant 1$. Other solutions are also possible, such as *over-damped modes*, with $\alpha = 0$ and non-oscillatory rapid decay ($\beta > 0$ but finite) and *critical modes* with frequency $\alpha \neq 0$ and $\beta \to +\infty$ ($\eta \to 1$) [12].

3. Influence of damping in simplified cable networks

A special case of a simplified cable network with limited number of independent variables is analyzed in this section to allow for the introduction and analysis of some basic characteristics that can be found in other examples and are useful in the understanding and interpretation of the mechanics of more realistic systems.

A set of two skew-symmetric cables (Fig. 2a) is interconnected by a vertical massless cross-tie, located at a distance l with respect to the left end of the upper reference stay. The total length of the upper cable is defined as L; the second one has an offset equal to l with respect to the reference abscissa and the right end with $l = l_{1,1}$ common to both segments 1,1 and 2,1 and $\xi = l/L$. The characteristics of the two stays are $H_1 = H_2 = H$ and $\mu_1 = \mu_2 = \mu$. Nodes $P_{1,1}$ and $P_{2,1}$ are connected by a linear spring of stiffness K. The infinite set of frequencies corresponding to individual-cable motion are $\alpha_{r1} = r$ and $\alpha_{r2} = r/(1-\xi)$, $r \in I^+$. The case study shown in Fig. 2(b) will be analyzed in the second part of this section.

In a first phase of this analysis, the damper is inactive ($c = 0$) and the resulting undamped network is considered, concentrating the study on the influence of the variable location ξ and the stiffness of the tie. The dimensionless parameter $d_K = H/KL$ is variable between 0 (rigid restrainer) and infinity (disconnected system).

Figs. 3(a1) and (a2) depict, as an example, the first and second modes corresponding to a case where $l = 0.20L$ and for $d_K = 1.0$ and extremely flexible connector. As a result, the first two frequencies $\alpha_1 = 1.024$ (cables in phase) and $\alpha_2 = 1.295$ (opposite-phase stays) are almost coincident with the fundamental modes of the independent stays 1 and 2 (i.e., $\alpha_{01} = 1.00$ and $\alpha_{02} = 1.25$), as also shown in Figs. 3(a1) and (a2). Results for

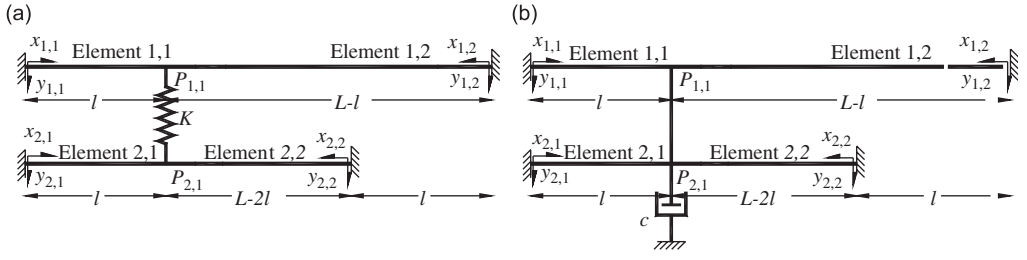

Fig. 2. Simplified networks-case studies: (a) skew-symmetric ($l_{22} = l_{11} = l$) two-stay network with flexible connector; (b) non-symmetric ($l_{22} = sl_{11}$, $s > 0$) two-stay network with rigid restrainer and damper to ground.

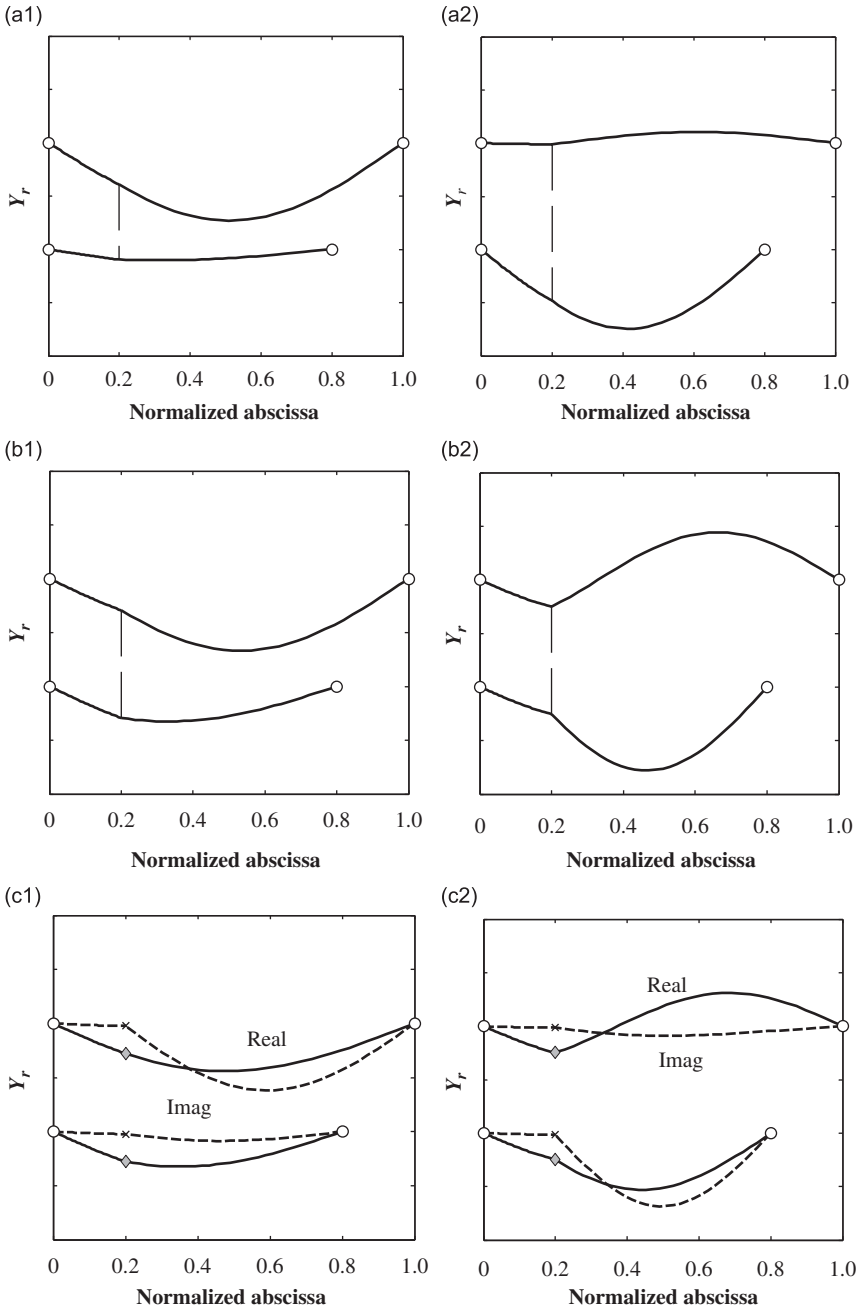

Fig. 3. Example of fundamental modes of the skew-symmetric network with $l = 0.2L$. First (a1: $\alpha = 1.024$) and second (a2: $\alpha = 1.295$) real eigen-solutions for $\rho = 0$ and flexible connection with $d_k = 1.0$; first (b1: $\alpha = 1.069$) and second (b2: $\alpha = 1.491$) real eigen-solutions for $\rho = 0$ and rigid connection with $d_k = 0$; first (c1: $\rho_{M1,\mathrm{Opt}} = 2.85$, $\gamma_{M1,\mathrm{Opt}} = 1.158 + 0.118\mathrm{i}$) and second (c2: $\rho_{M2,\mathrm{Opt}} = 3.48$, $\gamma_{M2,\mathrm{Opt}} = 1.569 + 0.115\mathrm{i}$) complex eigen-modes corresponding to optimal damping (real part, ——; imaginary part, – – –).

$d_k = 0$ and a perfectly rigid connection are shown in Figs. 3(b1) and (b2). The expected frequency up-shift is less evident for the first mode ($\alpha_1 = 1.069$) than for the second one ($\alpha_2 = 1.491$, Fig. 3b2), in which the opposite-phase behavior of elements 1,2 and 2,2 is responsible for a reduction of the effective wavelength; pseudo-symmetric (localized) modes [5] are also present (not shown). Enhancement in the performance is achieved for $0.2 < \xi < 0.3$, since the relative frequency increment between $d_k = 1.0$ and 0 is higher. More details can be found in Ref. [5].

In the second stage of the analysis (Fig. 2b) a damper linked to ground is installed in correspondence with node $P_{2,1}$ and a rigid tie is considered with $d_k = 0$. For practical applications, the assumption of "quasi-rigid" links among cables ($d_k \approx 0$) is usually acceptable [6]. The characteristic polynomial associated with $\det[\mathbf{S}] = 0$ becomes

$$p(\gamma\pi) = \sin(\gamma\pi\xi)\left\{\begin{array}{l}[2\cos(\gamma\pi\xi) + \mathrm{i}\rho\sin(\gamma\pi\xi)]\sin[\gamma\pi(1-\xi)]\sin[\gamma\pi(1-2\xi)] \\ \quad + \sin(\gamma\pi\xi)\sin[\gamma\pi(2-3\xi)]\end{array}\right\}. \tag{9}$$

The dimensionless damping parameter is defined as $\rho = c(H\mu)^{0.5}$. The first term of Eq. (9) is not influenced by the presence of the damper and corresponds to the set of purely real pseudo-symmetric modes with $\alpha_{PS,r} = r/\xi$, $r \in \Gamma^+$.

In the case of "locked-mode" real solutions (as $\rho \to \infty$) each element of the network is vibrating independently. Since $l_{1,1} = l_{1,2}$, repeated real eigen-values with multiple eigen-vectors are present, e.g., $\mathbf{\Phi}'_{L,Mu2} = [1,0,0,0]^T$ and $\mathbf{\Phi}''_{L,Mu2} = [0,0,1,0]^T$ for $\alpha_{L,Mu2} = r/\xi$.

Fig. 4(a) depicts the evolution of the complex frequency dependence on ρ for $l = 0.20L$. The figure presents the evolution curves for modes 1–6 (M1–M6), in which the complex roots are plotted for increasing values of damping in terms of normalized frequency α and damping ratio η. Different typologies of modes can be observed, similar to the regimes indicated in Ref. [12] for the case of a damper attached to a single stay. Modes 1–2 and 5–6 are typically underdamped and oscillatory; cross- and diamond symbols denote undamped and locked α_L solutions, respectively.

In Fig. 4(a) critical modes are present, emanating from the unrestrained oscillatory solution (cross-symbols, e.g., M2) and tending to a $\eta \to 1$ for $\rho \to \rho_{CR}$ ($\beta \to +\infty$ with $\alpha \neq 0$ finite). The quantity ρ_{CR} is a constant ($\rho_{CR} = 4.0$ in Fig. 4a), independent of the critical mode but a function of the network configuration (Section 4). Fig. 4(a) also shows the bifurcation for $\rho < \rho_{CR}$ between M3 and M4, possible since the critical frequency coincides with a single-multiplicity locked mode ($\alpha_L = 2.5 = \alpha_2$). Critical modes in simplified networks are usually related to vibration of shorter elements or portions of the network (i.e., segments 1,1 and 2,1 in Fig. 4a). More than one set of critical modes may be present, similarly to the case of two dampers on a single stay [21]. Fig. 4(b) shows another case of unanticipated behavior for $\xi = 0.45$ and $d_k = 0$ with multiple and partially overlapping frequency–damping trajectories for modes 4 and 5 (M4 and M5). Maximum damping is achieved for $\rho \cong 3.0$; the direction of increasing ρ is also indicated.

As an example of complex eigen-functions, Figs. 3(c1) and (c2) show real and imaginary parts of the mode shapes associated with the optimized modes $M1_{Opt}$ and $M2_{Opt}$ (maximum η) for $l = 0.2L$ and $d_k = 0$ in Fig. 4(a). While the real modal part is qualitatively the same as that observed with $c = 0$ (Fig. 3b1 and b2), the imaginary component (dashed line in Figs. 3c1 and c2) becomes significant for $M1_{Opt}$ and $M2_{Opt}$. This fact can

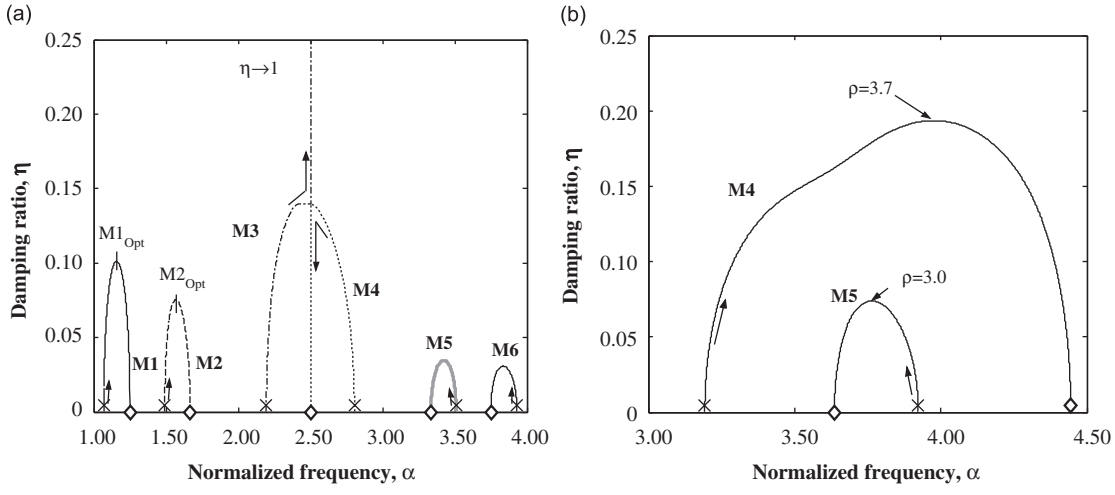

Fig. 4. Frequency–damping evolution curves of the simplified network with variable location (ξ) of the rigid cross-tie and $d_k = 0$. (a) Modes 1–6 (M1–M6) for $\xi = 0.20$, (b) multiple inner and outer branches for M4 and M5 with $\xi = 0.45$.

be interpreted by noticing that the imaginary eigen-function are mainly related to the first time derivative of y_{jp} and, therefore, predominantly influenced by the viscous absorber. In Fig. 3(c1) mode 1 is potentially "more dampable" ($M1_{Opt}$ with $\eta \cong 10\%$), in contrast with mode 2 (Fig. 3c2; $M2_{Opt}$ with $\eta < 10\%$) dominated by the opposing phases in elements 1,2 and 2,2.

4. Extension of the concept of "critical damping" to cable networks

In a generalized multistay cable network, where the installation of more restrainers will cause the presence of more solutions over a reduced frequency range, the derivation of the characteristic polynomial cannot be conducted analytically but numerically. However, for geometrically symmetric and simplified network, closed-form expressions for the critical damping can be found. In Fig. 5, a multistay parallel-cable symmetric network is considered, similar to the example studied in Section 4, in which the n cables have the same properties ($\omega_{01} = \omega_{0j} = \omega_{0n}$, $\gamma = \omega/\omega_{01} = \alpha + i\beta$), connected through a rigid and massless restrainer located at a distance l from the left-hand side of the system, with $\xi = l/L$. The components of the eigen-functions in Eq. (3) are defined as A_1, A_j, A_n (left-hand side) and $\hat{A}_1, \hat{A}_j, \hat{A}_n$ (right-hand side); $B_{j,p}$ are all zero due to the particular orientation of the local x–y axes. In the absence of damping ($\rho = 0$) the eigen-frequencies of the system are: (i) those of the disconnected cables with $\alpha \in I^+$ (no force through the restrainer), (ii) two classes of pseudo-symmetric frequencies for $\alpha_{PS,I} = r/\xi$ and $\alpha_{PS,II} = r/(1-\xi)$ with $r \in I^+$, each of which corresponds to a multidimensional eigen-vector subspace (all possible combinations of internal cables). For $\rho \neq 0$, the repeated application of Eq. (6) reveals that $A_1 = A_j = \cdots = A_n = A$ and $\hat{A}_1 = \hat{A}_j = \cdots = \hat{A}_n = \hat{A}$, provided that $\sin[\pi\gamma(1-\xi)] \neq 0$ and $\sin[\pi\gamma\xi] \neq 0$, i.e., excluding pseudo-symmetric modes. The system $\mathbf{S\Phi} = \mathbf{0}$ is characterized by two compatibility equations only with $\mathbf{\Phi} = [A, \hat{A}]^T$ and $\varepsilon = (1-2\xi)$,

$$A \sin[\pi\gamma\xi] - \hat{A} \sin[\pi\gamma(1-\xi)] = 0, \tag{10}$$

$$A[n \cos(\pi\gamma\xi) + i\rho \cos(\pi\gamma\xi)] + n\hat{A} \cos[\pi\gamma(1-\xi)] = 0. \tag{11}$$

The characteristic polynomial associated with Eqs. (10) and (11) becomes

$$p(\gamma) = n \sin(\pi\gamma) + 0.5i\rho[\cos(\pi\gamma\varepsilon) - \cos(\pi\gamma)]. \tag{12}$$

The real and imaginary parts of Eq. (12) with $\Theta = \pi\alpha$, $\Omega = \pi\beta$ must vanish, i.e.,

$$\mathrm{Re}_{p(\gamma)} = n \sin\Theta \cosh\Omega - 0.5\rho \sin\Theta \sinh\Omega + 0.5\rho \sin(\varepsilon\Theta) \sinh(\varepsilon\Omega) = 0, \tag{13a}$$

$$\mathrm{Im}_{p(r)} = n \cos\Theta \sinh\Omega - 0.5\rho \cos\Theta \cosh\Omega + 0.5\rho \cos(\varepsilon\Theta) \cosh(\varepsilon\Omega) = 0. \tag{13b}$$

The critical value of damping can be derived by recalling the definition of real overdamped modes [12,21] with $\Theta = \pi\alpha \equiv 0$. While Eq. (13a) becomes the null identity, the critical damping ρ_{CR} is obtained from

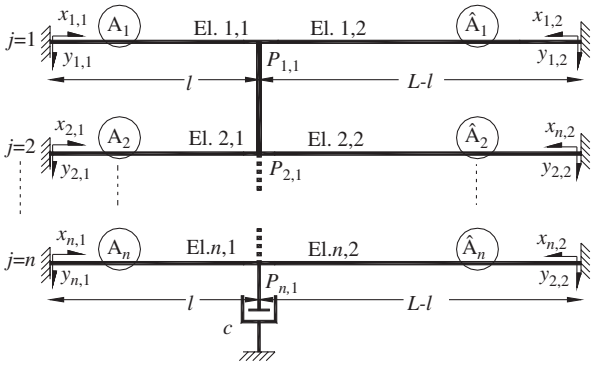

Fig. 5. Multistay parallel-cable symmetric network.

Eq. (13b) as $\Omega = \pi\beta \to \infty$ with $\varepsilon < 1$, i.e.,

$$\rho_{CR} = \lim_{\Omega \to +\infty} \rho(\Omega) = 2n. \tag{14}$$

Eq. (14) reveals that the critical value of the frequency for a multistay parallel-cable rigid-connector symmetric network is equal to twice the number of the stays and confirms the result observed in Section 3 for the system in Fig. 2. This equation can be interpreted a generalization of the individual-stay critical damping threshold [12] for the system in Fig. 5. For a real network, in which the tie flexibility, d_K, is responsible for relative displacement between the stays or multiple restrainers are present, Eq. (14) will also depend on d_K and, possibly, on the mass of the connectors $M_{j,p}$. In these cases a numerical solution of the system $\mathbf{S}(\Theta,\Omega,\rho)$ can be implemented for $\Theta = 0$ and the condition

$$\lim_{\Omega \to +\infty} \det[\mathbf{S}(\Theta = 0, \Omega, \rho)] = \det[\lim_{\Omega \to +\infty} \mathbf{S}(\Theta = 0, \Omega, \rho)] = 0. \tag{15}$$

The interchange between the limit and the determinant operators in Eq. (15) is possible since the limit of the matrix functional $\mathbf{S}(\Theta, \Omega, \rho)$, as $\Omega \to +\infty$, exists and is finite. Eq. (15) is scalar and complex as a function of ρ only; similarly to Eqs. (13a) and (13b), inspection reveals that the real part of this equation is identically zero, while the imaginary part converges to ρ_{CR} (numerically, for large Ω).

5. Case study: the Fred Hartman Bridge

5.1. Use of transverse cross-ties for vibration mitigation purposes

The presented results are related to the application of the methodology to the study of the side-span unit of the south tower of the Fred Hartman Bridge [6], a twin-deck cable-stayed bridge over the Houston Ship Channel, with central span of 380 m and side spans of 147 m. The current configuration of the "A-line" 12-stay system (side span, south tower) is shown in Fig. 6(a). Before cross-ties were installed in 1998, large-amplitude vibration was often observed in the stays. For this reason the original 12-stay configuration was modified by means of three transverse restrainers as in Fig. 6(a), an "eight-loop" steel wire rope system. In the figure, the proposed retrofit with the addition of external dampers is also indicated; dampers are denoted as D1 and D2.

Physical properties and geometry of each cable were specified in accordance with the original design specifications and adjusted using relevant measurements. The equivalent model, used in the simulations, is depicted in Fig. 6(b) (units in meters). Cable AS1 is considered as reference: $f_{01} = \omega_{01}/2\pi = 0.626$ Hz. Each cross-tie is simulated by appropriately calibrated linear springs. The original configuration, currently installed on the Fred Hartman Bridge, does not include mechanical dampers.

In the case of a cable network without external devices for energy dissipation, the solution to the in-plane free-vibration problem was derived in Ref. [6] and two types of modes were identified: *global network modes* with significant increment of modal mass, usually the fundamental ones, where all cables are active and a large number of *localized modes* related to narrow frequency intervals, where selected *jp* elements only contribute to the vibration, linked to all the combinations of internal segments of the network.

It is convenient to express the system performance in terms of two dimensionless groups $\rho_{D1} = c_{D1}/(\mu_1 H_1)^{0.5}$ and $\rho_{D2} = c_{D2}/(\mu_1 H_1)^{0.5}$, where c_{D1} and c_{D2} represent the viscous damping coefficient of the two devices, μ_1 and H_1 the mass and tension of the reference cable (AS1).

5.2. Analysis of the cable network with the addition of one external damper connected to the deck

The introduction of a single damper (D1) in correspondence with Restrainer 3 of the "A-line" was first considered. The Frequency–damping evolution as a function of ρ_{D1} (with $\rho_{D2} = 0$) is depicted in Fig. 7(a) for the fundamental modes (M1–M3, for α between 1.0 and 4.0) and Fig. 7(b) for some of the localized modes (M5–M7, in the range $3.72 < \alpha < 3.80$). All the investigated modes have an origin at the undamped solution corresponding to the current configuration of the network, labeled as "uu" in the figure (cross-symbols in Fig. 7b), and they all belong to the category of complex underdamped modes, as described in Section 3. The direction of increasing damping is also indicated with the locked-frequency nodes labeled as "ru" (diamond symbols in Fig. 7b).

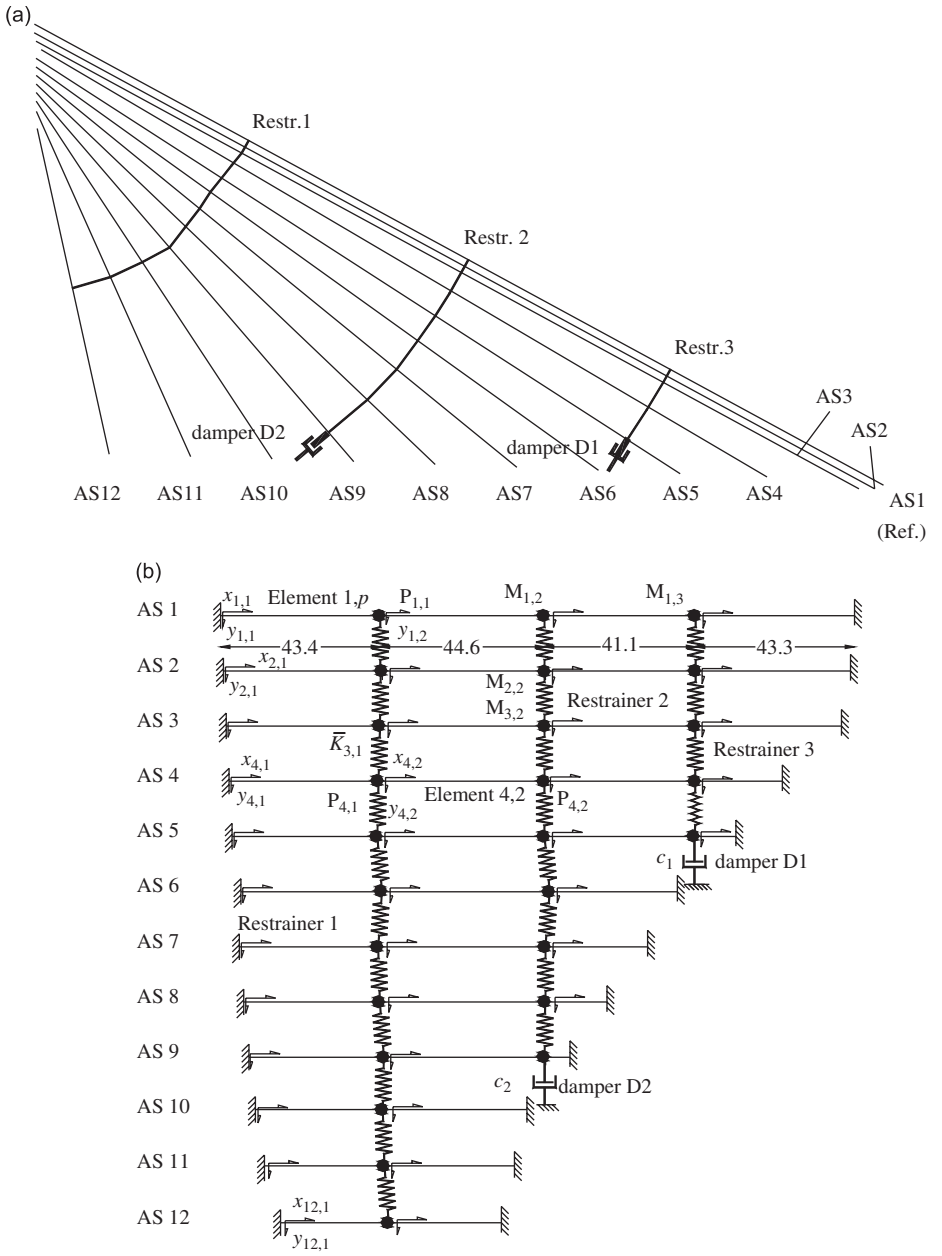

Fig. 6. Fred Harman Bridge ("A-line"): (a) 3D network, (b) equivalent model.

Some of the characteristics of these curves are similar to the simplified network case studied in Section 3, as for M1 in Fig. 7(a), between nodes M1uu and M1ru. Mode 4 (localized solution) was omitted from Fig. 7(b) since its evolution was very similar to M5. Some differences can be observed for modes M2 and M3. A distinction with respect to the case of an individual taut cable is the fact that the number of solutions increases and several real roots can coexist in the limiting cases of $\rho_{D1} = 0$ and $\rho_{D1} \to \infty$ in a reduced range of frequencies. Critical damping was numerically computed through the procedure described in Section 4 and estimated as $\rho_{\mathrm{CR},D1} \cong 4.3$.

Comparison of Fig. 7(a) with Fig. 7(b) reveals that global modes are mainly affected by the installation of the damper (M1–M3), while localized eigen-functions are practically unaltered (M5–M7). In the latter case

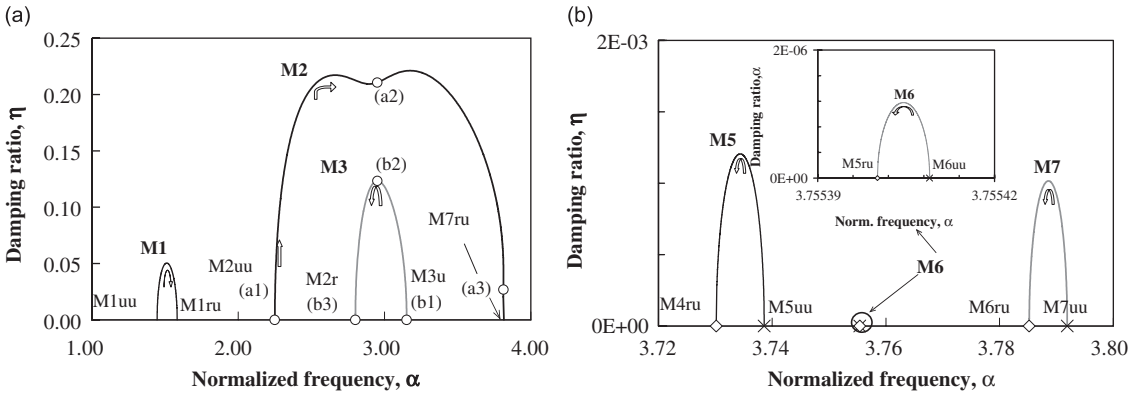

Fig. 7. Frequency–damping evolution curves of the "A-line" with the addition of damper D1: (a) fundamental modes, M1–M3, (b) localized modes (M5–M7). Arrows show direction of increasing damping; the nodes indicating "*u*" correspond to $\rho_{D_p} = c_{D_p}(H_1\mu_1)^{-0.5} = 0$, "*r*" to $\rho_{D_p} \to \infty$ with $p = 1,2$.

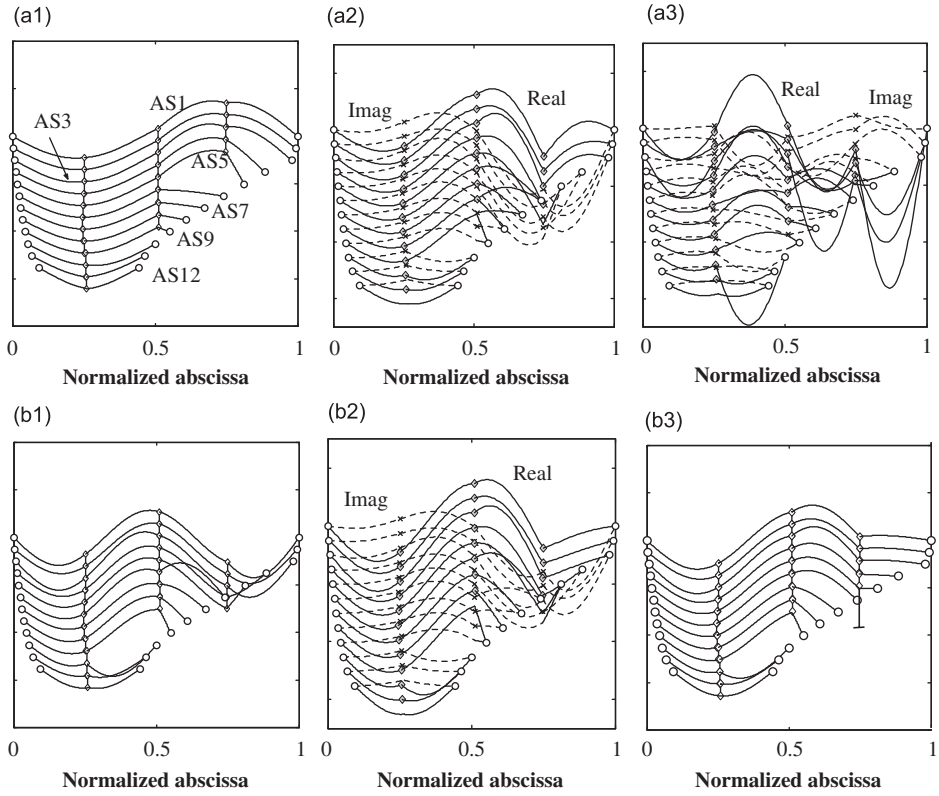

Fig. 8. Evolution of the eigen-solutions of the "A-line" with the addition of damper D1. Mode 2: (a1) $\rho_{D_p} = 0.00$, $\alpha = 2.25$ (M2uu, real), (a2) $\rho_{D_p} = 7.14$, $\gamma = 2.95 + 0.64$i, (a3) $\rho_{D_p} = 39.04$, $\gamma = 3.81 + 0.10$i. Mode 3: (b1) $\rho_{D_p} = 0.00$, $\alpha = 3.15$ (M3uu, real), (b2) $\rho_{D_p} = 7.06$, $\gamma = 2.95 + 0.37$i, (b3) $\rho_{D_p} \to \infty$, $\alpha = 2.80$ (M2ru, locked).

(Fig. 7b), insignificant values of damping ratios are achieved (less than 0.2%) due to the fact that modal amplitudes in correspondence with the external node of Restrainer 3 are limited.

A peculiar set of solutions can be observed in Fig. 7(a), with the simultaneous presence of outer (M2) and inner (M3) trajectories, partially overlapping without crossing. This particular type of solution is the extension of the behavior depicted in Fig. 4(b) for simplified networks (Section 3). This trend was studied in detail in

terms of complex eigen-functions associated with these two modes, as depicted in Figs. 8(a1)–(a3) for mode 2 and Figs. 8(b1)–(b3) for mode 3. The scale used in these pictures is arbitrary; these modes correspond to the special nodes (circle symbols) in Fig. 7(a).

Mode 2 evolves from the second mode of the original configuration (M2uu in Fig. 8a1), progresses to a high-damping (21%) solution (Fig. 8a2, $\rho_{D1} = 7.14$) and subsequently migrating to a frequency range typical of localized modes (M7ru as $\rho_{D1} \to \infty$).

In Fig. 8(a3), the complex eigen-function, evaluated at $\rho_{D1} = 39.04$ is shown ($\gamma = 3.81 + 0.10\mathrm{i}$) with $\eta \cong 2.5\%$, with transition to a localized mode. Modal amplitudes have been scaled in the plots to highlight the contributing elements. This behavior has been interpreted by recalling the fact that the "A-line" network can be divided in two regions: stays AS1–AS5, directly affected by the damper, and the remaining cables, simply driven by this mechanism. The active cables (AS1–AS5) tend to behave as a "generalized" solution of the single cable-damper example [12], with the device located at a distance of 0.15–0.25 dimensionless units from the idealized right end. Three concurring phenomena are believed to contribute to the evolution of mode 2: a lower modal compatibility of M2uu with respect to M2ru, the observation that in the case of the "locked network" with $\rho_{D1} \to \infty$ a fundamental anti-symmetric mode disappears from the category of global modes (M1ru, M2ru only are global in comparison with M1uu, M2uu, and M3uu) and the absence of critical solutions for this range of frequencies, since primarily associated with shorter network elements (Section 3).

It must be observed that the force equilibrium in correspondence with Restrainer 3 in Figs. 8(a2), (a3) and (b2) with $\rho_{D1} \neq 0$ must be interpreted as a combination of real and imaginary parts, apparently violated if either contribution is only considered.

In contrast, mode 3 evolves backwards on the frequency axis from M3uu with real $\alpha = 3.15$ in Fig. 8(b1) to an intermediate complex eigen-solution ($\gamma = 2.95 + 0.37\mathrm{i}$, $\rho_{D1} = 7.06$) at the same frequency as M2 but with considerably lower damping (12%, Fig. 4b2), and subsequently decreasing to the second mode of the network with locked damper to ground as $\rho \to \infty$, M2ru (Fig. 8b3). The evolution of M2 and M3 can be interpreted by recalling that the frequency of both undamped and locked solutions such as, for example, M3uu and M2ru for M3, can be associated with a characteristic global network wavelength and cannot change significantly during the migration between the two cases.

In Figs. 8(a2) and (b2), the presence of modes with the same α and inner and outer loops is physically possible due to the similarity with Fig. 4(b). The significant differences in the maximum attainable damping ratio (21% and 12%, respectively, corresponding to distinct ρ_{D1}) can be related to the different magnitudes of the complex part of the eigen-solution for stays AS1–AS5, in correspondence with the damper location.

In general, it was concluded that Damper D1 is capable of considerably improving the response for mode 2 and in part for mode 3, as shown in Fig. 7(a) ($\eta > 10\%$ in both modes). From the design point of view, an optimal unit for the anti-symmetric mode 2 ($\eta = 21\%$, $\rho_{D1} = 7.14$) corresponds to $c_{D1} \approx 150\,\mathrm{kN\,s/m}$. Moreover, low damping ratios (5%) in the fundamental mode can be achieved, since the location of damper D1 is unfavorable. In general, the damper coefficient, c, corresponding to maximum η is different for M1 and M3, suggesting that simultaneous optimal performance is impossible in the presence of a single external unit.

5.3. *Analysis of the cable network with the addition of multiple dampers*

In this section, the simultaneous presence of dampers D1 and D2 (Figs. 6a and b) is considered. Critical damping in the presence of both D1 and D2 was numerically computed (Section 4) under the assumption of equal units, $\rho_{D1} = \rho_{D2}$. The numerical solution indicated two independent values of critical damping, $\rho_{\mathrm{CR},D1} \cong 4.3$, coincident with the quantity derived in Section 5.2 for single unit, and $\rho_{\mathrm{CR},D2} \cong 3.1$. This fact suggests that, as shown for an individual cable [21], if $\rho_{D1} = \rho_{D2}$ the behavior of the two units is independent at critical conditions, i.e., the critical eigen-function is concentrated in the proximity of either damper, and that $\rho_{\mathrm{CR},D1}$ and $\rho_{\mathrm{CR},D2}$ may be different for a network.

As a first example, the optimization of mode 1 only is considered with $\rho_{D1} \neq \rho_{D2}$. From the optimal node "M1ou" $\rho_{D1}^{\mathrm{Opt}} = 6.10$, corresponding to a damper coefficient c_{D1} approximately equal to 128 kN s/m as shown in Fig. 9(a) by a thin line and circle symbol, the second damping parameter was progressively incremented from $\rho_{D2} = 0$. The thick line of Fig. 9(a) shows the solution for this new configuration, originating from the reference point "M1uo" and progressively reaching a new maximum at $\rho_{D2} = 7.95$, equivalent to a damper

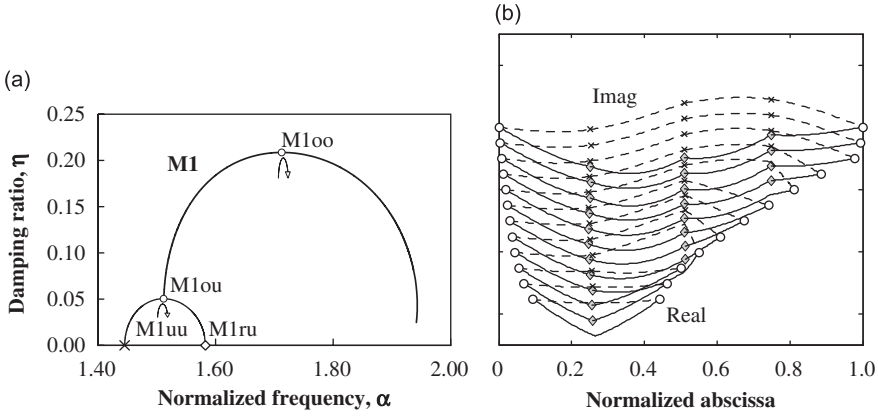

Fig. 9. First-mode optimal damping ("A-line") in the presence of dampers D1 and D2: (a) frequency–damping evolution curve (——, damper D1 only; ——, D1 and D2 dampers), (b) first-mode complex eigenfunction of the optimized system (M1oo node): $\rho_{D1} = 6.10$, $\rho_{D2} = 7.95$, $\gamma = 1.71 + 0.37i$.

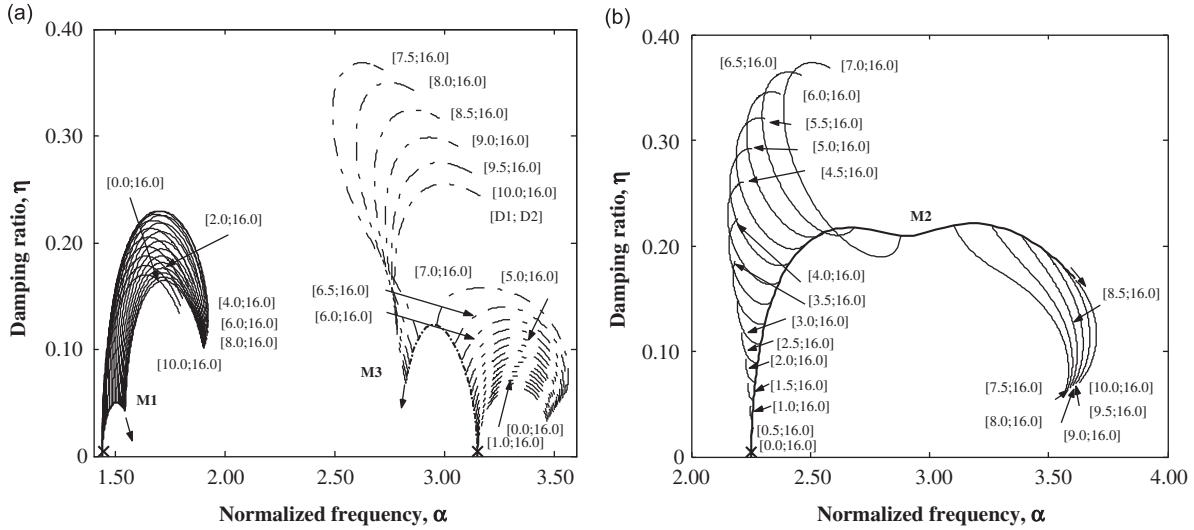

Fig. 10. Frequency–damping curves (α–η) of the "A-line" with two dampers, D1 and D2, for $0 < \rho_{D1} < 10$ and $0 < \rho_{D2} < 16$ ($\rho_{D_p} = c_{D_p}(H_1\mu_1)^{-0.5}$, $p = 1,2$): (a) Modes 1 (M1) and 3 (M3), (b) mode 2 (M2).

with $c_{D2} = 169\,\text{kN s/m}$, denoted by "M1oo" in the figure. The corresponding complex eigen-mode ($\rho_{D1}^{\text{Opt}} = 6.10$, $\rho_{D2}^{\text{Opt}} = 7.95$, $\gamma = 1.71 + 0.37\text{i}$) can still be classified as underdamped (Fig. 9b); the performance is excellent ($\eta > 20\%$) due to the favorable location of damper D2 close to mid-span.

A second control strategy was explored in order to identify optimized solutions for multiple modes, in particular for modes 1 (M1) and 3 (M3). Frequency–damping curves were numerically generated for M1 and M3 by simultaneously varying ρ_{D1} and ρ_{D2} in the intervals $0 < \rho_{D1} < 10$ and $0 < \rho_{D2} < 16$. The upper limits of these intervals were decided a priori by considering the potentially large dimensions of these devices. In Fig. 10(a), a collection of these two classes of α–η evolution curves is depicted (solid lines for M1, broken lines for M3). Every curve in Fig. 7(a) has origin from the "backbone lines" with $\rho_{D2} = 0$ and is numerically computed by progressively varying ρ_{D2} with given constant ρ_{D1}. For each of these branches, the end node in Fig. 10(a) is accompanied by the notation $[\rho_{D1},\ \rho_{D2\max}]$ with $\rho_{D2\max} = 16.0$. It is worth noticing that the extension of these curves to $\rho_{D2} \to \infty$ does not correspond to a real mode due to $\rho_{D1} \neq 0$ but finite.

For M1 an increase of ρ_{D2} is always associated with a monotonic increment of both α and η. In contrast, the evolution of M3 is more articulated in the presence of the second damper; as an example, a backward/forward frequency trajectory originating from the backbone is observed for $\rho_{D1} > 7.0$ (Fig. 10a).

The evolution of mode 2 was separately analyzed in Fig. 10(b), for the same interval of ρ_{D1} and ρ_{D2}. The backbone curve for $\rho_{D2} = 0$ is represented by a thick solid line. In Section 5.2, a transition from global skew-symmetric mode to localized solution was recorded in the absence of D2 for increasing values of ρ_{D1}. As a results, if the complex mode is global and dominated by a skew-symmetric configuration such as, for example, for $\rho_{D1} < 3.0$ in Fig. 10(b), the introduction of the second device in correspondence of a nodal point of the network (Fig. 8a1) produces no significant increment of η. For intermediate values $3.0 < \rho_{D1} < 7.5$, the influence of the second damper is more evident as shown on the upper left-hand side of Fig. 10(b); the numerical procedure also suggests a decrement of η with respect to the backbone curve for M2 such as, for example, $\rho_{D1} = 7.0$ and $\rho_{D2} > 0$. For $\rho_{D1} = 7.5$, corresponding to the evolution to a localized mode (Section 5.2), the addition of the second device accelerates this transition (right-hand side of Fig. 10b).

From the collection of the solutions presented in Fig. 10(a) for modes M1 and M3 iso-damping contours were generated, by reordering the normalized damping parameters, ρ_{D1} and ρ_{D2}, under the condition of constant η. Fig. 11(a) depicts the ρ_{D1}–ρ_{D2} contours for $\eta = 10\%$, 15%, 20% for both M1 (solid lines, with progressively increasing thickness) and M3 (dashed lines). For M1 the iso-curves are closed circuits with progressively reduced size, whereas V-shaped irregular patterns are evident for M3. The mutual intersection of the η-equivalent contours associated with M1 and M3, defines the condition of uniform damping for both eigenvalues, i.e., a condition of equivalent simultaneous optimization of the network in different modes. In Fig. 11(a), the nodes "ID_{10}" ($\eta = 10\%$) with $\rho_{D1} = 5.3$ and $\rho_{D2} = 2.0$, and "ID_{15}" ($\eta = 15\%$) with $\rho_{D1} = 6.9$ and $\rho_{D2} = 4.2$, are shown. The latter case can be translated into $c_{D1} \approx 145\,\mathrm{kN\,s/m}$ and $c_{D2} \approx 90\,\mathrm{kN\,s/m}$, corresponding to large units but still acceptable from the design perspective. This is a significant advantage of the multiple-damper configuration with respect to single-damper network, where one mode at a time can only be optimized.

Iso-damping contours can also be plotted for M2 (Fig. 11b); the curves are not continuous due to the articulated behavior of this mode. From the analysis of Figs. 10(b) and 11(b) it was also concluded that M2 is not of concern in the regimes corresponding to $4.0 < \rho_{D1} < 7.5$ and nodes "ID_{10}" and "ID_{15}" for the investigated case, since the damping ratio exceeds 15% independently of ρ_{D2}. Nevertheless, it must be observed that, in general, the proposed multimode optimization procedure may possibly require the analysis of iso-damping curves including all fundamental modes, i.e., M1–M3.

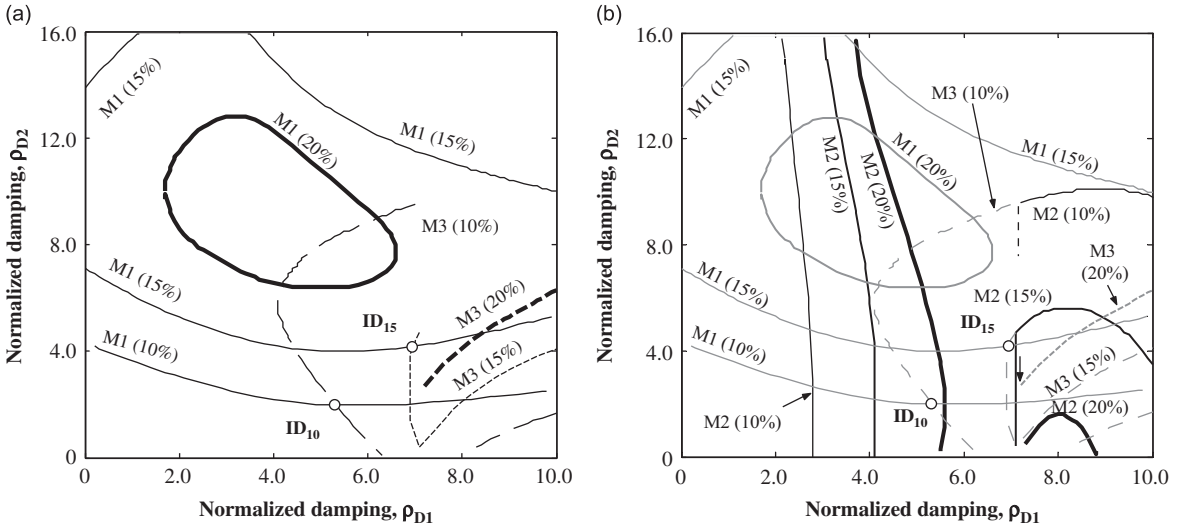

Fig. 11. Iso-damping contours of the "A-line" global modes with two dampers, D1 and D2, as a function of ρ_{D1} and ρ_{D2} ($\rho_{D_p} = c_{D_p}(H_1\mu_1)^{-0.5}$, with $p = 1,2$) and damping ratio $\eta = 10$, 15, and 20%: (a) modes M1 and M3 only, (b) modes M1, M2 and M3.

The design of the wire ropes can be addressed by analyzing the expected modal axial internal forces on the transverse elements, as suggested in a previous study [19], in particular for the fundamental global modes. In general, when a damper to ground is introduced in correspondence with a restrainer, a significant increment in the axial force of the restrainer segments is recorded. As an example, in Fig. 8(b3) a 40% increase of axial force in Restrainer 3 was observed if the ground connector was included with respect to Figs. 8(b1) and (a1). Large relative increments must be avoided due to the possibility of slackening/snapping of the wire ropes.

Finally, it is worth mentioning that the derivation of asymptotic solutions for small frequency shift for cable networks, similar to design curves for an individual stay, was recently explored in Ref. [22]. The comparison of the predictions with the numerically generated solution was reasonable; however, derivation of a unique and simple relationship, applicable to a wide range of cases and capable of representing the dynamics of a multistay damped network, did not seem practical and the use of such curves could not fully replace the complete dynamic analysis.

6. Conclusions

The problem of in-plane large-amplitude oscillation mitigation of cable networks was presented and examined through an analytical technique founded on the linear taut-cable theory. This problem is of particular significance for the retrofit of inclined stays of cable-stayed bridges often affected by vibration associated with wind and wind–rain excitation.

A hybrid passive control strategy, in which the transverse restrainers of the interconnected network system are combined with linear dampers connected to the deck, was developed. An analytically based and numerically implemented methodology in the complex domain was considered, allowing for the free-vibration analysis in the presence of energy dissipation devices.

Analytical solutions derived for a simplified damped network, also reported herein, and the collection of observations from the free-vibration behavior of a taut-cable with two dampers [21] have contributed to the identification and interpretation of the in-plane dynamic behavior of large multiple-stay multiple-damper networks such as, for example, inter-related solution patterns and the modal evolution for different classes of eigenvalues. The results have shown that even the study of a geometrically simple system can become challenging in terms of number and type of solutions.

The main part of this research was concentrated on the investigation of the performance of a real network example (Fred Hartman Bridge, Houston, TX, USA) in relation to both fundamental and higher modes, and their evolution as a function of the amount of damping that is introduced. The improvement of the response that is achieved by carefully considering more than one passive device connected to the network at the deck level was also evaluated.

The efficacy of the proposed hybrid method can be primarily associated with global modes, for which the dampers are fully active and provide a significant contribution to energy dissipation. Advantages of this solution with respect to the more common mitigation solution of a damper installed on an individual stay include the fact that the location of the unit is not geometrically restricted to the cable ends due to presence of the deck. In fact, this location can be selected in accordance with the position of the cross-ties along the network, in particular where modal displacements of the undamped eigen-solutions are usually larger, clearly enabling a more efficient structural control. Moreover, it has been shown that the use of more than one damper on a cable network at the same time is preferable due to the possibility of multiple-mode optimization. This opportunity is usually unattainable in more traditional configurations, in which the optimal damping can only be referred to one mode in particular.

Localized modes, in which only the internal portion of the system is responding, tends to be marginally affected by the presence of external dampers and may become potential vulnerable to externally induced oscillation. Although these modal solutions usually correspond to a less critical higher frequency range, vibration problems cannot be excluded and need consideration. A possible solution associated with the introduction of dampers at internal locations only between two consecutive stays, although not directly discussed in this paper, can be found in Ref. [19].

Out-of-plane vibration control in the case of a cable network is less manageable due to the fact that the influence of the restrainers is minimal in the transverse direction. Although in most cases network-type

systems have been demonstrated efficient in the vibration reduction, this is an inherent limitation of all cross-tied systems for the case of wind-induced oscillation with non-negligible out-of-plane component. Analysis of the trajectories of unrestrained individual cables, observed in the field, are typically elliptical with major axis inclined with respect to the in-plane direction [1]. This observation indicates a complex mechanism depending on the three-dimensional orientation of the stays with respect to the wind direction, and is not currently considered by the proposed formulation.

Acknowledgments

This research has been supported in part through an FHWA-sponsored project (Harold Bosch technical contact) on stay-cable vibration awarded to a team of investigators including HNTB Corporation, New York, Johns Hopkins University, Baltimore, MD, Rowan Williams, Davies and Irwin, Ontario, Canada, Buckland and Taylor of Vancouver, BC, Canada. The Fred Hartman and Veterans' Memorial Bridges Project has been funded by the Texas Department of Transportation through Texas Tech University and the University of Texas at Austin. The first author would like to acknowledge the support of Northeastern University, start-up funding for new faculty members.

This material is also based in part upon work supported by the National Science Foundation under Grant no. 0305903. This support is gratefully acknowledged. Any opinions, findings, and conclusions or recommendations expressed in this material are those of the author(s) and do not necessarily reflect the views of the National Science Foundation, the Texas Department of Transportation and the United States Department of Transportation, Federal Highway Administration.

References

[1] D. Zuo, N.P. Jones, The mechanism of rain–wind-induced vibration: vortex-shedding or galloping, *Proceedings of the 10th Americas Conference on Wind Engineering*, Baton Rouge, LA, USA, May 31–June 4, 2005, CD-ROM.

[2] H. Yamaguchi, H.D. Nagahawatta, Damping effects of cable cross ties in cable-stayed bridges, *Journal of Wind Engineering and Industrial Aerodynamics* 54–55 (1995) 35–43.

[3] H. Yamaguchi, M. Alauddin, Control of cable vibrations using secondary cable with special reference to nonlinearity and interaction, *Engineering Structures* 25 (6) (2003) 801–816.

[4] M. Virlogeux, Cable vibrations in cable-stayed bridges, in: A. Larsen (Ed.), *Bridge Aerodynamics*, A.A. Balkema, Rotterdam, NL, 1998, pp. 213–233.

[5] L. Caracoglia, N.P. Jones, In-plane dynamic behavior of cable networks, part 1: formulation and basic solutions, *Journal of Sound and Vibration* 279 (3–5) (2005) 969–991.

[6] L. Caracoglia, N.P. Jones, In-plane dynamic behavior of cable networks, part 2: prototype prediction and validation, *Journal of Sound and Vibration* 279 (3–5) (2005) 993–1014.

[7] T.J. Carne, *Guy Cable Design and Damping for Vertical Axis Wind Turbines*, Sandia National Laboratories, SAND80-2669, 1981.

[8] H.M. Irvine, *Cable Structures*, MIT Press, Cambridge, MA, USA, 1981.

[9] B.M. Pacheco, Y. Fujino, A. Sulekh, Estimation curve for modal damping in stay cables with viscous damper, *Journal of Structural Engineering* 119 (6) (1993) 1961–1979.

[10] Z. Yu, Y.L. Xu, Non-linear vibration of cable-damper systems, part I: formulation, *Journal of Sound and Vibration* 225 (3) (1999) 447–463.

[11] Y.L. Xu, Z. Yu, Non-linear vibration of cable-damper systems, part II: application and verification, *Journal of Sound and Vibration* 225 (3) (1999) 465–481.

[12] J.A. Main, N.P. Jones, Free vibrations of a taut cable with attached damper. I: linear viscous damper, *Journal of Engineering Mechanics—ASCE* 128 (10) (2002) 1062–1071.

[13] S. Krenk, Vibrations of a taut cable with external damper, *Journal of Applied Mechanics—Transactions of the ASME* 67 (4) (2000) 772–776.

[14] S. Krenk, J.R. Høgsberg, Damping of cables by a transverse force, *Journal of Engineering Mechanics—ASCE* 131 (4) (2005) 340–348.

[15] E.A. Johnson, R.E. Christenson, B.F. Spencer Jr., Semiactive damping of cables with sag, *Computer-aided Civil and Infrastructure Engineering* 18 (2) (2003) 132–146.

[16] C.S. Cai, W.J. Wu, X.M. Shi, Cable vibration reduction with a hung-on TMD system, part I: theoretical study, *Journal of Vibration and Control* 12 (7) (2006) 801–814.

[17] H.R. Bosch, S.W. Park, Effectiveness of external dampers and crossties in mitigation of stay cable vibrations, *Proceedings of the Sixth International Symposium on Cable Dynamics*, Charleston, South Carolina, USA, September 19–22, 2005, CD-ROM.

[18] C.N. Jensen, S.R.K. Nielsen, J.D. Sorensen, Optimal damping of stays in cable-stayed bridges for in-plane vibrations, *Journal of Sound and Vibration* 256 (3) (2002) 499–513.

[19] L. Caracoglia, N.P. Jones, Selection of an optimized cable network system configuration, *Proceedings of the 17th ASCE Engineering Mechanics Conference*, University of Delaware, Newark, DE, USA, June 13–16, 2004, CD-ROM.

[20] L. Sun, C. Shi, H. Zhou, Y. Zhou, Vibration mitigation of long stay cable using dampers and cross-ties, *Proceedings of the Sixth International Symposium on Cable Dynamics*, Charleston, South Carolina, USA, September 19–22, 2005, CD-ROM.

[21] L. Caracoglia, N.P. Jones, Damping of taut-cable systems: multiple dampers on a single stay, *Journal of Engineering Mechanics—ASCE* 33 (10) (2007).

[22] L. Caracoglia, N.P. Jones, Design of mitigation devices for stay-cable vibration, *Proceedings of the Sixth International Symposium on Cable Dynamics*, Charleston, South Carolina, USA, September 19–22, 2005, pp. 125–132.